Vortex Induced Vibrations of a U-beam under two different flow patterns

Johannes Strecha* and Herbert Steinrück*
*Institute of Fluid Mechanics and Heat Transfer, Vienna University of Technology, Vienna, Austria

Summary. The aero-elastic properties of a slender U-beam are investigated for flow velocitys ranging from the vortex excitation velocity upwards. Two different flow patterns, related to the behaviour of the free shear layer above the cavity of the U were found to give rise to completely different vibration phenomena. While one flow pattern can lead to pronounced vortex-induced vibrations, self-excited flutter vibrations were observed under the other flow pattern. A comparison with wind tunnel experiments is given.

Introduction

We investigate vortex-induced two-degree of freedom (vertical or "heave", and torsional or "pitch") vibrations of a slender U-beam (frontal height H and width B, see figure 1b) with a specific aspect ratio, at a Reynolds number of magnitude 10^5 by means of CFD simulations. Interesting phenomena arise as it was found that the flow around the U-beam can take on two different patterns, significantly influencing its aero-elastic properties.
Originally, the aero-elastic stability of a tensioned, slender U-shaped belt was investigated. The belt, as indicated in figure 1a, is subject to steady wind blowing normal to its long axis with a low turbulence intensity at a velocity u_∞. The construction of the belt is such that only vertical (heave) and torsional (pitch) motion are possible. Motivated by the design of the belt, we assume that the respective eigenfrequencies are of similar magnitude and that the cross-section of the belt is not deformed by its motion. The horizontal (swaying) motion is considered to be much smaller than the heave and pitch motion. Thus, it is neglected in the following. We consider mode 1 vibrations of a section of the belt with a length $l \gg (H, B)$ with clamped ends.
Therefore, the belt is modeled as a two-dimensional U-profile in parallel turbulent flow with velocity u_∞. The U-profile supported by linear springs (see figure 1b). It has two degrees of freedom, heave y and pitch φ. The ratio of eigenfrequencies $\Omega = f_{0,\mathrm{y}}/f_{0,\varphi}$ shall be $\Omega = 1$. The aspect ratio of the frontal height H and the belt width B is $B/H = 4.65$. The Reynolds number $\mathrm{Re} = u_\infty B/\nu_{\mathrm{Air}}$ is of the magnitude $\mathrm{Re} \sim 10^5$ here. The vortex shedding behind the U-profile occurs at a frequency f_{vs} and is used to calculate the Strouhal number $\mathrm{St} = Hf_{\mathrm{vs}}/u_\infty$. By simulations we found that $\mathrm{St} \approx 0.135$ for the stationary profile. The investigated dimensionless reduced velocities $U_\infty = u_\infty/(Hf_0)$ range from $U^* = 1/\mathrm{St} \approx 7.4$ where vortex induced vibrations are expected, to $U^* \gtrsim 30$.
The force and moment coefficients are given by $F = \boldsymbol{c}_{\mathbf{F}} \cdot \frac{1}{2}\rho_{\mathrm{air}} u_\infty^2 H$ and $M = \boldsymbol{c}_{\mathbf{M}} \cdot \frac{1}{2}\rho_{\mathrm{air}} u_\infty^2 HB$, respectively where F and M are the aerodynamic forces and moments of torsion per unit length.

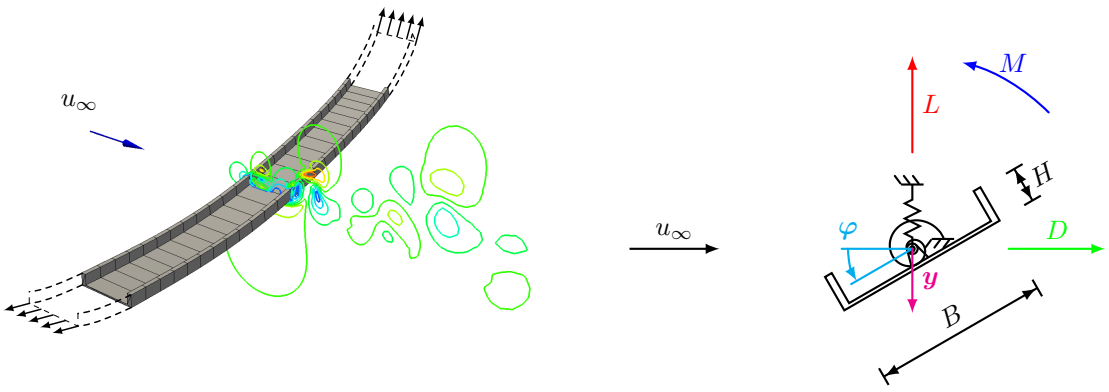

(a) Sketch of the tensioned U-beam in wind.

(b) Two-dimensional model of the U-beam supported by linear springs. The aerodynamic forces lift L, drag D and torsional moment M act on the profile.

Figure 1: Vertical (heave) and torsional (pitch) vibrations of a slender U-beam in cross flow are investigated.

The flow around the U-profile and its motion is investigated by means of two-dimensional CFD simulations and accompanying wind tunnel experiments.
In the following section the setup of the simulation and the wind tunnel experiments is described.

Methodology: Simulations and wind tunnel experiments

The simulations were carried out using the proprietary finite volume CFD solver ANSYS FLUENT version 14.5. An unsteady-RANS (URANS) model (i.e. the kω-SST turbulence model) is employed to model the turbulent aspects of the

flow. This choice for the simulation setup is deemed suitable for studies of the qualitative behaviour of the U-profile. The quantitative results should be viewed critically. Comparison with wind tunnel experiments is sought to verify the simulation results.
To allow for motion of the U-profile a part of the mesh has to be deformed. Here, an approach inspired by [1] was chosen: An annulus shaped region (see figure 2) connects the inner region of the mesh, which moves with the rigid U-profile, to the stationary, outer region. Thus, the mesh close to the profile need not be deformed.

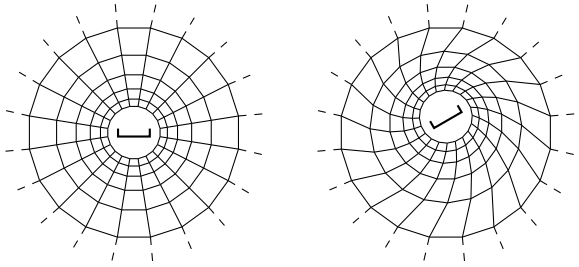

(a) Initial mesh (b) Deformed mesh

Figure 2: Mesh deformation strategy to accommodate the moving U-profile. The annulus is embedded in a rectangular computational domain.

The segregated approach (iterative coupling), imposed by the choice of a proprietary CFD solver could be used successfully since the density of the U-beam (originally made of rubber) is much greater than the density of air.
To integrate the equations of motion for the U-profile (rigid body motion) a fourth order Runge Kutta scheme is used. This requires an estimate of the time-dependent aerodynamic forces. This estimate is obtained from the partially converged flow-field several times throughout the solution process (i.e. employing the concept of so-called *stagger iterations*) to avoid numeric instabilities.

Wind tunnel experiments: Test stand
The wind tunnel experiments were carried out at the the *Centre of Excellence Telč* (CET) where a special test-stand is available: It allows rigid section models to rotate and vertically translate. The respective eigenfrequencies can be adjusted individually. The test-stand uses Evans linkage to allow vertical motion of the model and an auxiliary linkage to support rotation of the model (see figure 6a). It is described in more detail in [3].

Two flow patterns

In this section the two time periodic patterns of the flow around the stationary U-profile are described in more detail. Both flow patterns were observed in CFD simulations on very fine calculation meshes for extended periods of flow-time. We consider the angle of inclination φ as selection mechanism. Note, that in this section $y \equiv 0$ and $\varphi = const.$ Free vibrations are considered in the next section.
The fundamental difference between the two flow patterns lies in the behaviour of the free shear layer, separating from the U-profile at its top windward corner. This shear layer can either be curved weakly, giving rise to what will be called "R-flow" pattern in the following, or it can roll up quickly, reaching into the cavity of the U-profile, giving rise to the so-called "U-flow" pattern.
When the R-flow is realized the free shear layer is curved weakly and extends into the wake behind the U-profile (see figure 3b). Vortices form behind the U-profile with the frequency f_{vs}. The flow is very similar to the flow around a full rectangular prism with equal aspect ratio (hence the name "R-flow"). The stationary vortex in the cavity of the U-profile corresponds to the closed wall of the rectangular prism. The aerodynamic forces acting on the profile vary sinusoidally with the vortex shedding frequency f_{vs} (see figure 3a).
When the U-flow is realized the free shear layer is rolling up right behind the windward sidewall of the U-profile (see figure 4b, vortex $\boldsymbol{L}$). This creates a large instationary vortex and a secondary vortex ($\boldsymbol{S}$) which separate from the sidewall and are advected through the cavity of the U-profile. Although additional vortices are formed in the wake behind the U-profile the dominant contribution to the aerodynamic forces is the "collision" of the large vortices $\boldsymbol{L}$, with the leeward sidewall. This happens at a frequency of about, but not exactly $f_{\mathrm{vs}}/2$, which is reflected in the aerodynamic forces (see figure 4a). Note, that we associate f_{vs} with the R-flow pattern only.
In the literature, it can be found that the shear layers separating from a short rectangular prism (B/H small) behave similar, [9]. CFD simulations of the flow around the prism showed, that the shear layers originating from the corners of the prism also can roll up either strongly or weakly. In this case, however, the flow patterns change intermittently and the strong and weak shear layer roll up is reflected in large and small fluctuations of the aerodynamic lift force, explaining older wind tunnel experiments, see figure 13a in [6].
As mentioned before, whether the U-flow or the R-flow is realized depends on the angle of inclination φ. Maintaining a positive inclination "helps" the U-flow to develop. Negative inclinations, however, lead to the R-flow pattern. Around a

certain angle $\varphi \approx 2°$ both flow patterns can be realized and sustained for extended periods of flow time.
In case of the R-flow the time-averaged lift is higher than when the U-flow is present (see figure 5a). The oscillations of the lift around its time average is more pronounced when the U-flow is realized.
The different vortex configurations in either flow pattern also influence the fundamental frequency of the aerodynamic forces. In case of the R-flow the fundamental frequency can be used to calculate a meaningful Strouhal number (see figure 5b). The fundamental frequency in case of the U-flow is no longer related to the vortex formation in the wake and thus should not be used to calculate a Strouhal number. Instead, the second harmonic is related to the vortex shedding in the wake.

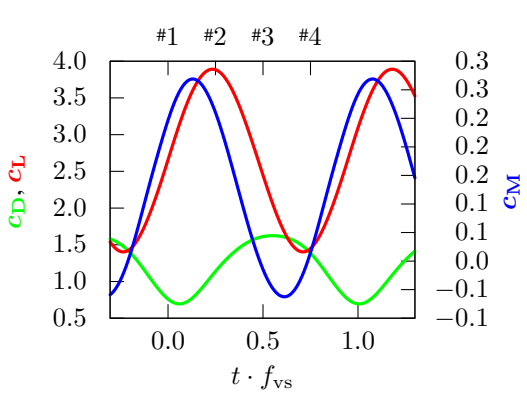

(a) Time-periodic aerodynamic forces acting on the U-profile.

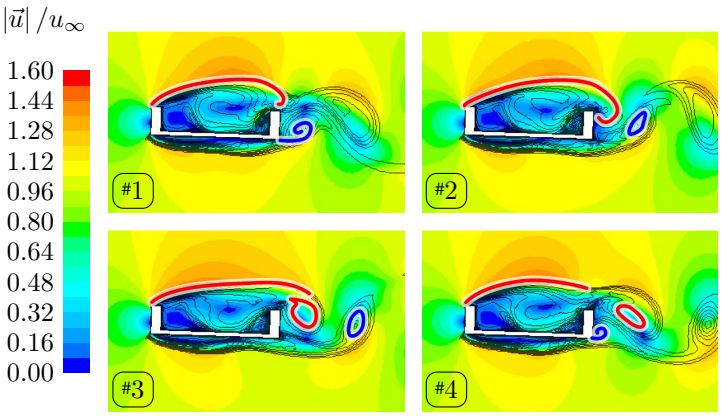

(b) Snapshots of the flow field, coloured by the velocity magnitude with vorticity magnitude isolines.

Figure 3: Characteristic features of the R-flow. Simulation at $\mathrm{Re} = 2.45{\cdot}10^5$.

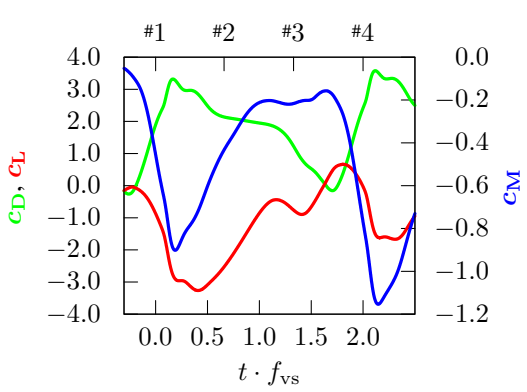

(a) Time-periodic aerodynamic forces acting on the U-profile.

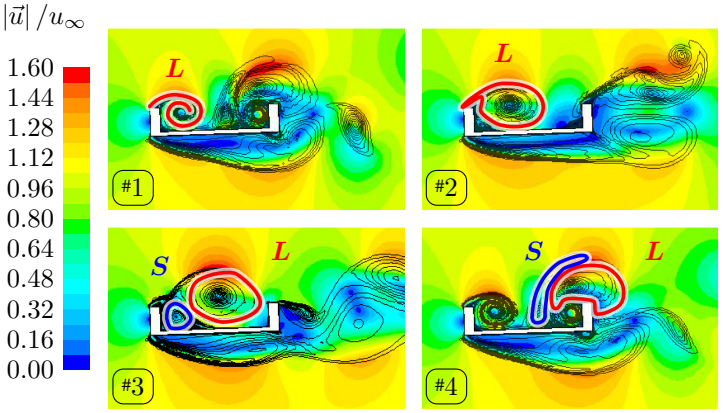

(b) Snapshots of the flow field, coloured by the velocity magnitude with vorticity magnitude isolines.

Figure 4: Characteristic features of the U-flow. Simulation at $\mathrm{Re} = 2.45{\cdot}10^5$.

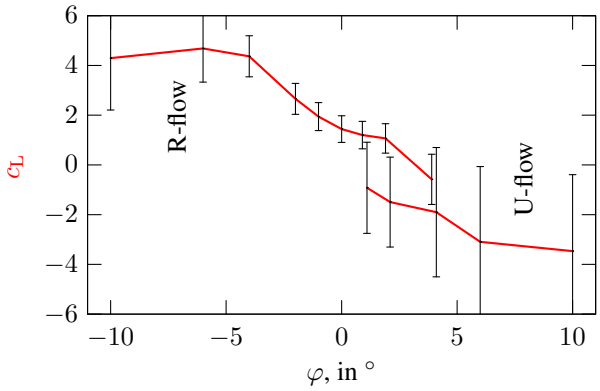

(a) Coefficient of Lift c_L. Continuous line: time average, bars: half of the oscillation amplitude around the time-average.

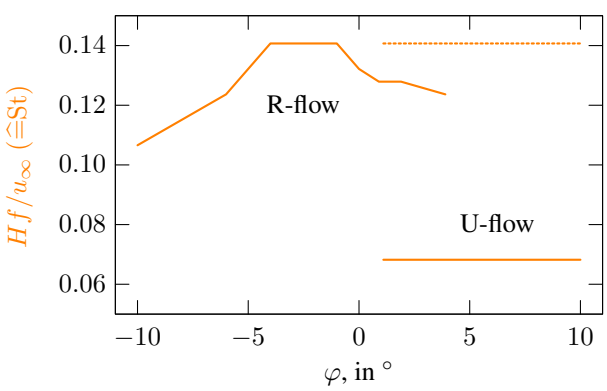

(b) Scaled fundamental frequency (continuous line) of the aerodynamic forces. Dashed line: second harmonic.

Figure 5: Lift coefficient and fundamental frequency of the aerodynamic forces for several angles of inclination.

Vibrations

In this section the different aero-elastic properties under the U-flow and R-flow patterns are discussed. The vibration amplitudes will be quantified by the root mean square (R.M.S.) value of the mean-free data (e.g. $\sum_i[(y_i - \bar{y})^2 / N]$ where $\bar{y}$ is the average of the samples y_i) over a suitable time interval and the absolute maximum value in this interval (e.g. $\max |y_i - \bar{y}|$).
In the wind tunnel experiments self-excited vibrations at larger reduced velocities ($U^* \approx 30$) could be observed. At these reduced velocities the section model carried out flutter vibrations. Both degrees of freedom were excited (see figure 6b).

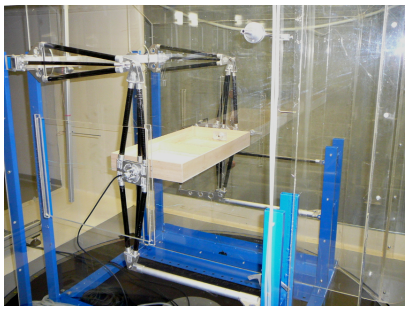

(a) Photography of the test-stand with the mounted section model (see also [3])

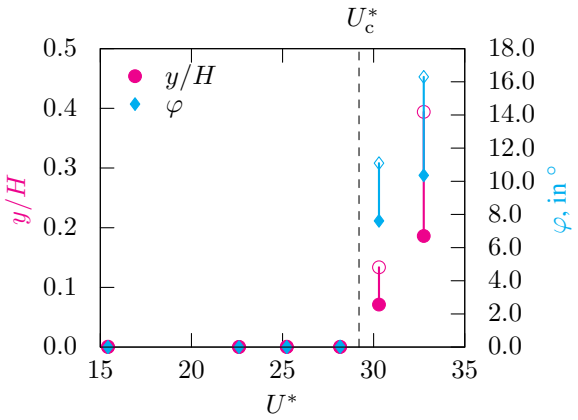

(b) R.M.S. (full symbol) and maximum (open symbol) values of the dimensionless heave and pitch for large reduced velocities, $\Omega = 1.0$ and $\varphi_0 = 0°$.

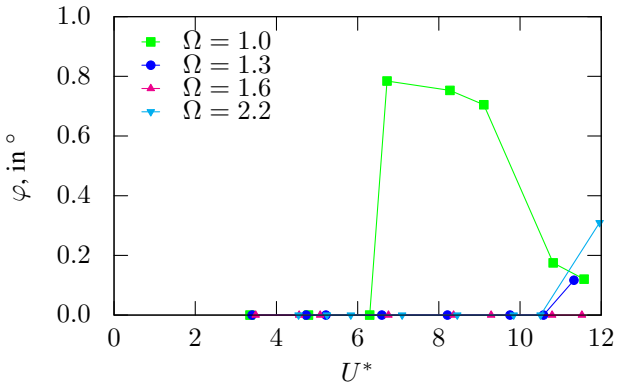

(c) R.M.S. pitch for low reduced velocities and several frequency ratios at $\varphi_0 = 0°$.

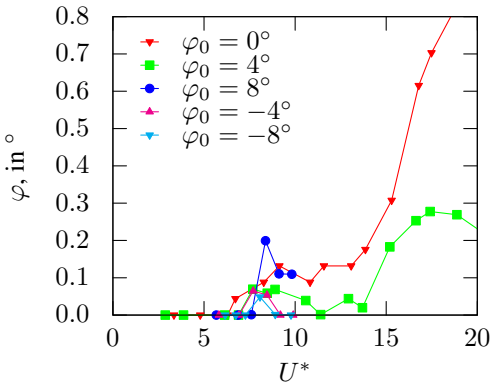

(d) R.M.S. pitch for low reduced velocities and several initial angles of inclination φ_0 at $\Omega = 1.0$.

Figure 6: Wind tunnel experiments: Measured vibration amplitudes for various reduced velocities.

At lower reduced velocities in the range of $U^* \approx 1/\mathrm{St}$ only very small vibration amplitudes could be observed. Clearly, these vibrations were related to the vortex shedding behind the section model. This is consistent with simulations of the vibrations under the R-flow pattern. Changing the eigenfrequency ratio and the equilibrium angle of attack φ_0 did not lead to more pronounced vibrations (see figure 6d).
A simulation of the R-flow resonance case ($U^* = 7.4$) also shows very small vibrations (see figure 7a). An explanation for the small amplitudes could be found by inspecting the spectra of the aerodynamic forces. The simulation of the resonance case was set up such that the eigenfrequency of the profile equals the fundamental frequency of the lift force of the stationary U-profile. Surprisingly, the fundamental frequency of the lift force changed to a lower value (see figure 7b) in free vibration simulations! Thus, due to the motion of the profile, the state of resonance could not be reached. Matsumoto, [5] and Manzoor, [4], reported similar observations.
If the U-flow is initially present the resonance case is no longer at $U^* = 7.4$ but at $U^* \approx 14.0$, corresponding to $U^* = 1/\mathrm{St}$ and $U^* \approx 2/\mathrm{St}$ under the R-flow pattern. In contrast to the R-flow resonance case, large amplitude vibrations dominated by the pitch motion could be observed in a simulation at $U^* = 14.0$ and below (see figure 8). The heave motion is comparatively small in this range. The saturated vibration amplitudes increase from $U^* \approx 8$ to $U^* = 14$. This contrasts measurements of vibrations of a rectangular prism by M. Matsumoto, [5], where the model was at relative rest at $U^* = 14$. This emphasizes once more the particularity of the U-profile under the U-flow pattern.
At $U^* = 14$ pitch vibrations with a large amplitude $\hat{\varphi} \approx 11°$ set in during the first few vibration periods (see figure 9a). After an initial transient phase the pitch amplitude remains approximately constant throughout the simulated flow time.

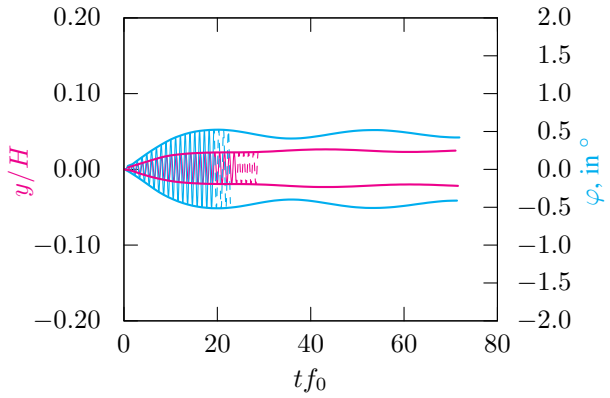

(a) Dimensionless heave and pitch amplitudes.

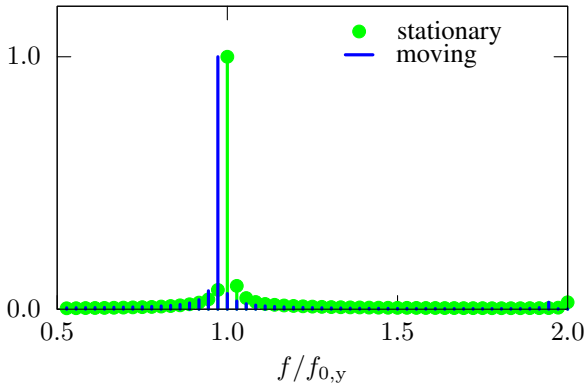

(b) Power density spectra of the lift force for the stationary U-profile and simulated free vibration at $U^* = 1/\mathrm{St}$, normalized by the respective maximum.

Figure 7: Simulation of the R-flow resonance case ($U^* = 1/\mathrm{St}$), $\mathrm{Re} = 4.45{\cdot}10^5$ and $\Omega = 1.0$.

The heave amplitude remains at comparatively low $\hat{y}/H \approx 0.05$.
At $U^* \approx 16$ the initial heaving motion becomes more important than at lower reduced velocities $U^* < 16$. But this heaving motion appears to be incompatible with the U-flow pattern. The flow changes to the R-flow pattern! Subsequently, the vibrations appear to die out. In case of $U^* = 16$ this apparently takes a very long time (downward pointing arrow in figure 8). At larger reduced velocities $16 < U^* \lesssim 30$ simulations confirmed that (i) the flow changes to the R-flow pattern after an initial transient phase and (ii) that the initially excited vibrations die out.
At higher reduced velocities the R-flow pattern itself can give rise to flutter vibrations, as seen in the wind tunnel experiments. In the simulations, which were carried out without structural damping, this leads to very large amplitudes (see figure 9b) which ultimately cause the calculation mesh to become invalid.

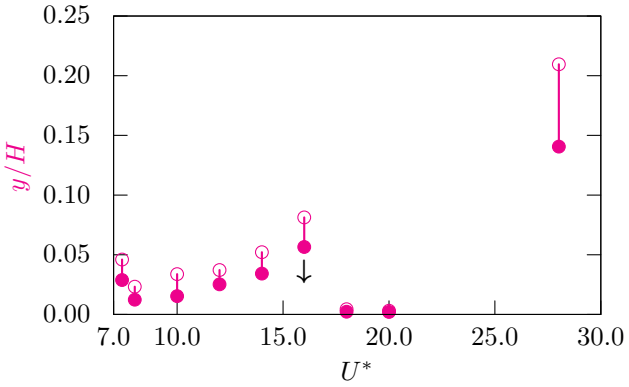

(a) Heave y.

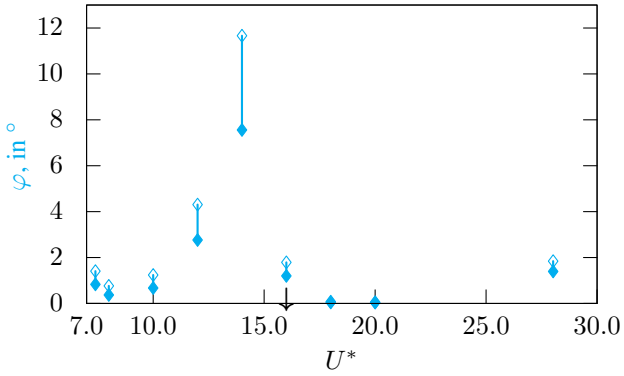

(b) Pitch φ.

Figure 8: Simulation under the U-flow pattern: R.M.S. and maximum values of the vibration amplitude for several reduced velocities.

Conclusions

The aero-elastic properties of the U-beam greatly depend on the flow pattern. The R-flow permits self-excited vibrations at $U^* \gtrsim 30$. The linear method of aerodynamic derivatives (see [8]) could be applied, which is part of the ongoing research. More recently, modeling coupled mode flutter is addressed in [7]. At higher reduced velocities the U-flow pattern cannot persist (at least in the simulated case of vanishing structural damping) since the the flow changes to the R-flow pattern due to the initial heaving motion of the profile.
At lower reduced velocities no (vortex-induced) vibrations could be observed under the R-flow pattern. The fundamental frequency of the aerodynamic forces under the R-flow pattern is given by the vortices forming in the wake of the U-profile. Thus, they depend on a characteristic width of the wake which, in turn, appears to depend on the profile motion.
In contrast to this, pronounced vibrations were observed under the U-flow pattern, but at a reduced velocity of $U^* \approx 14$ (instead of $U^* = 7.4$ in classical vortex-induced vibrations). Here, the fundamental frequency of the aerodynamic forces under the U-flow depends on the time the vortex separating from the front wall of the U takes to reach the rear wall, which appears not to depend on the profile motion. In this sense it is plausible that the U-flow admits more pronounced vibrations than the R-flow.

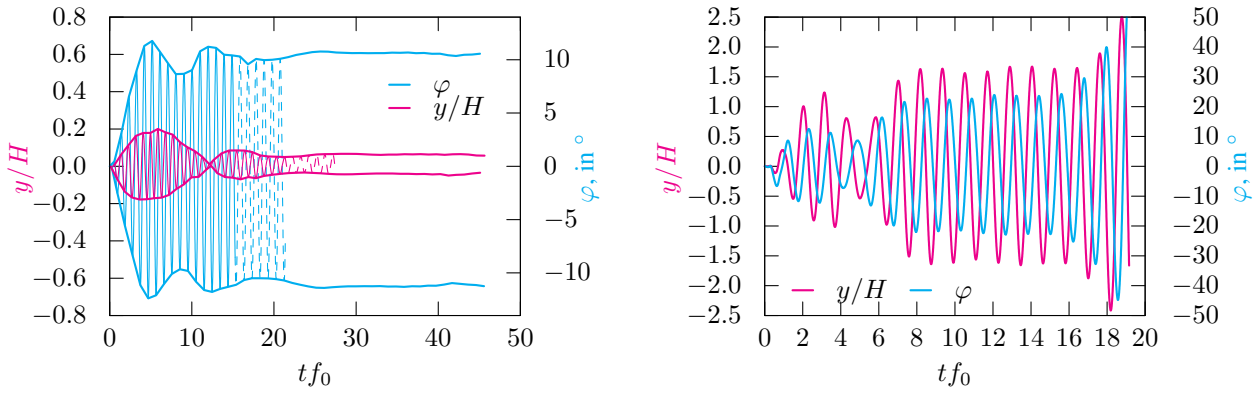

(a) $U^* = 14.0$. (b) $U^* = 32.0$.

Figure 9: Simulation under the U-flow pattern: Oscillation amplitudes of the heave y and pitch φ for two reduced velocities.

It should be noted that as of the time of writing vibrations under the U-flow pattern could only be observed in simulations and (allegedly) in the field, but not in wind tunnel experiments. To design new experiments that favour the U-flow pattern and employ flow visualization techniques is part of the ongoing research.
However, the evolution of vortices can be highly three-dimensional, as is commonly known. This three-dimensional evolution is not or poorly captured by two-dimensional or three-dimensional URANS simulations ([2]), respectively. Although [1] had some success with three-dimensional URANS simulations we feel that future research should employ Large Eddy Simulation techniques.

References

[1] Bai, Y., Sun, D., Lin, J. (2010) Three dimensional numerical simulations of long-span bridge aerodynamics, using block-iterative coupling and DES. *Computers & Fluids* **39**:1549–1561.

[2] Fröhlich, J., von Terzi, D. (2008) Hybrid LES/RANS methods for the simulation of turbulent flows. *Progress in Aerospace Sciences* **44**:349–377.

[3] Král, R., Pospíšil, S., Náprstek, J. (2013) Experimental Set-up for Advanced Aeroelastic Tests on Sectional Models. *Experimental Techniques.* doi: 10.1111/ext.12056.

[4] Manzoor, S., Khawar, J., Sheikh, N. A. (2013) Vortex-Induced Vibrations of a Square Cylinder with Damped Free-End Conditions. *Advances in Mechanical Engineering* **2013**:1–12.

[5] Matsumoto, M., Yagi, T., Tamakic, H., Tsubota, T. (2008) Vortex-induced vibration and its effect on torsional flutter instability in the case of B/D = 4 rectangular cylinder. *Journal of Wind Engineering and Industrial Aerodynamics* **96**:971–983.

[6] Nakamura, Y., Matsukawa, T. (1987) Vortex excitation of rectangular cylinders with a long side normal to the flow. *Journal of Fluid Mechanics* **180**:171–191.

[7] Náprstek, J., Pospíšil, S. (2012) Response types and general stability conditions of linear aero-elastic system with two degrees-of-freedom. *Journal of Wind Engineering and Industrial Aerodynamics* **111**:1–13.

[8] Scanlan, R. H., Tomko, J. J. (1971) Airfoil and Bridge Deck Flutter Derivatives. *Journal of the Engineering Mechanics Division* **97**:1717–1737.

[9] Tamura, T., Itoh, Y. (1999) Unstable aerodynamic phenomena of a rectangular cylinder with critical section. *Journal of Wind Engineering and Industrial Aerodynamics* **83**:121–133.